Hindawi
Journal of Engineering
Volume 2020, Article ID 7063243, 12 pages
https://doi.org/10.1155/2020/7063243

Review Article

Optimization of an On-Grid Inverter for PV Applications Using Genetic Algorithms

Anis Ammous, Abdulrahman Alahdal, and Kaiçar Ammous

Department of Electrical Engineering, CEIA, Umm Al Qura University, Makkah, Saudi Arabia

Correspondence should be addressed to Kaiçar Ammous; ammous.kaissar@gmail.com

Received 4 December 2019; Accepted 21 February 2020; Published 30 March 2020

Academic Editor: YoungSu Yun

A new approach to the optimal design of power inverters for on-grid photovoltaic systems that uses genetic algorithms (GA) is provided in this article. The nonlinear average model is adopted to model the conversion stage in order to accurately evaluate and quickly estimate the power losses of the power devices. The hysteresis current control that guarantees a quasi-sinusoidal output current is applied to generate the inverter control signals. The design of the solar inverter must meet three contradictory objectives that need to be optimized at the same time. In fact, the aim is to maximize the efficiency of the converter while minimizing its size and price under electrical constraints. The problem variables are the output current ripple and the passive and active components available on the market (IGBTs/MOSFETs, Diodes, Inductors). NSGA-II (Elitist Nondominated Sorting Genetic Algorithm) is appropriate in the case where discrete design variables are used to search for optimal Pareto solutions. It carries out a systematic and efficient search among the developed databases for a set of components which define the optimal structures of the inverter. The introduced method makes the design task easier since the best solutions depend on the components available on the market and significantly reduces the time to market for manufacturers.

1. Introduction

According to the BP Statistical Review of World Energy [1], global energy demand has increased by 2.9% in 2018, nearly twice the average annual growth in demand over the past decade (+1.5%/year) and the fastest since 2010. At this unprecedented increase, a strong growth in the integration of renewable energy sources into power plants worldwide has been recorded [2–9]. Thus, progressive advances of renewable energy power generation systems have led to the search for solutions to improve the performances of these systems, mainly by taking advantage of the enormous developments in the power semiconductor industry. In fact, power electronics are at the core of power generation systems since they provide the technology between sources and loads that converts energy from its continuous form into alternative or inverse [10]. Recently, photovoltaic (PV) electrical power generation has become more and more visible because it is a very attractive way to produce energy for several reasons, especially for its simplicity and modularity. It is almost entirely in solid form from the PV cell to the generated electricity. Whether it is a power plant with less than 1 W or a 100 MW grid-connected one, all that is needed between the solar system and the load are electronic and electrical components. Compared to other energy sources that humanity has used to produce electricity for a long time, PV is the most flexible and modular. Large PV systems require more electric buses, fuses, and wiring, but the most crucial component between the solar panel and the load is the electronic component that converts and processes electricity: it is the inverter [11, 12].

One approach widely adopted for improving the entire grid-connected PV system performances is upgrading the converter by acting on its own design or on its control strategy or on both by benefiting from optimization algorithms as efficient and commonly used tools to obtain the best possible converter [13–16]. The design, control, and performance problems encountered in the field of power electronics generally involve the simultaneous optimization of multiple objectives which are often in contradiction (e.g.,

the simultaneous minimization of the power losses and the design cost or volume). In order to resolve conflicts, these cases can be formulated as multiobjective optimization problems.

This paper describes a methodology for designing grid-connected PV inverters that optimizes efficiency and/or volume and/or price, taking into account the quality of output current and the maximum switching frequency of active devices and based on commercially available components. This approach simplifies the implementation phase of the optimal solution since it is based on what we have on the market.

The next part highlights the modeling process of the studied system, shown in Figure 1, by using the nonlinear averaged model with discrete semiconductor devices and the hysteresis current control. In the third part, the non-dominated sorting genetic algorithm NSGA-II as well as the method used to determine the optimal solution is investigated. The fourth part presents the process used to manipulate the genetic algorithm with discrete variables and defines the design parameters, the constraints, and the fitness of optimization problems. Then, optimization results and interpretations are provided and finally, conclusions are given.

2. DC/AC Converter Modelling

2.1. Nonlinear Average Model with Discrete Semiconductor Devices. Modeling and dynamic simulation are essential tools to analyze, design, control, and optimize a power electronics structure. Averaging techniques are well used to model power converters since it ensures both accuracy and rapidity, two criteria that must always be met while modeling power systems especially when dealing with multiobjective optimization problems. The average model of power electronic devices is a simplified presentation of a switching cell that is common in several converter topologies [17, 18]. Nonlinear effects of the power semiconductor devices are not included in most of averaged models because they use ideal switches instead of semiconductor device models. Considering the unsatisfactory situation in the averaged modeling, an effort was undertaken in the averaged models presented in [19–21]. Thus, the authors have proposed an advanced PWM-switch model including semiconductor device nonlinearities.

Figure 2(a) presents the inverter leg to be modeled with two complementary transistors (IGBTs or MOSFETs) controlled by external gate signals and two freewheeling diodes. In Figure 2(b), the equivalent representation of power converter leg using averaged model is illustrated. In fact, upper switches are replaced by a controlled voltage source V_1 while lower ones are substituted by a controlled current source I_1 given by

$$\begin{aligned} V_1 &= \langle U_{as} \rangle, \\ I_1 &= \langle i_{e2} \rangle. \end{aligned} \tag{1}$$

The main advantage of the proposed nonideal average model is to supply accurate losses values with acceptable simulation costs. The power losses of semiconductors ($P_{\text{transistor}}$ and P_{diode}) comprising conduction and switching losses and taking into account the various conduction and switching times are derived from switching characteristics of power devices presented in Figure 3 and can be given by [20, 21]

$$\begin{aligned} P_{\text{transistor}} = {} & \frac{I_L V_t}{T_s}\left(\rho T_s - t_{\text{don}} - t_r - t_{rr} + t_{\text{doff}}\right) \\ & + \left(\frac{V_b - E - V_d}{3T_s} + \frac{E + V_d}{2T_s}\right)\left(I_L + I_{\text{RM}}\right)\left(t_r + t_{\text{IRM}}\right) \\ & + \left(\left(\frac{V_b - V_t}{3T_s} - \frac{V_b}{2T_s}\right) I_{\text{RM}} + \left(\frac{V_t - V_b}{2T_s} + \frac{V_b}{T_s}\right)\right. \\ & \left. \cdot \left(I_{\text{RM}} + I_L\right)\right)\left(t_{rr} - t_{\text{IRM}}\right) \\ & + \frac{E + V_d - V_t}{2T_s} I_L t_{rv} + \frac{V_t}{T_s} I_L t_{rv} + \frac{E + V_d + V_L}{2T_s} \\ & \cdot \left(I_L + X I_{\text{queue}}\right) t_{fi} \\ & + \frac{E + V_d}{2T_s} X I_{\text{queue}} t_{\text{queue}}. \end{aligned} \tag{2}$$

$$\text{With } X = \begin{cases} 0 & \text{if the transistor is a MOSFET} \\ 1 & \text{if the transistor is an IGBT} \end{cases}$$

$$\begin{aligned} P_{\text{diode}} = {} & \frac{I_L V_d}{T_s}\left(T_s - \rho T_s + t_{\text{don}} - t_{\text{doff}} - t_{fi} - t_{rv} + t_{\text{don}}\right) \\ & + \frac{I_{\text{RM}}}{2T_s}\left(V_L + V_{L1} - V_d\right)\left(t_{rr} - t_{\text{IRM}}\right) \\ & + \frac{I_{\text{RM}}}{6T_s}\left(V_b - V_t\right)\left(t_{rr} - t_{\text{IRM}}\right) + \frac{I_L V_d}{2T_s} t_{fi} - \frac{I_{\text{RM}}}{2T_s} V_d t_{\text{IRM}}. \end{aligned} \tag{3}$$

$T_s = 1/f_s$ is the switching frequency.

To perform average model simulations with discrete semiconductor devices, it is crucial to determine the static and dynamic characteristics of each component. For that, the determination of the model parameters is done using the technical data sheets of the semiconductor devices and based on study developed in [22].

2.2. Hysteresis Current Control. Hysteresis control is one of the simplest nonlinear mechanisms to ensure spontaneous current regulation in power systems [23, 24]. It will directly define the state of the switches in the H-bridge topology to track the output current I_{out} to its reference I_{ref} with a fixed value for the current ripple given by ΔI. The band delimited by $(I_{\text{ref}} \pm \Delta I)$ is called the hysteresis band and any violation of these two limits results in a change of power switch state from conduction to blocking or vice versa. Figure 4 reveals the principle of this control strategy where the on-time T_{on} and off-time T_{off} depends on the sign of grid voltage V_s and the output voltage V_{out}.

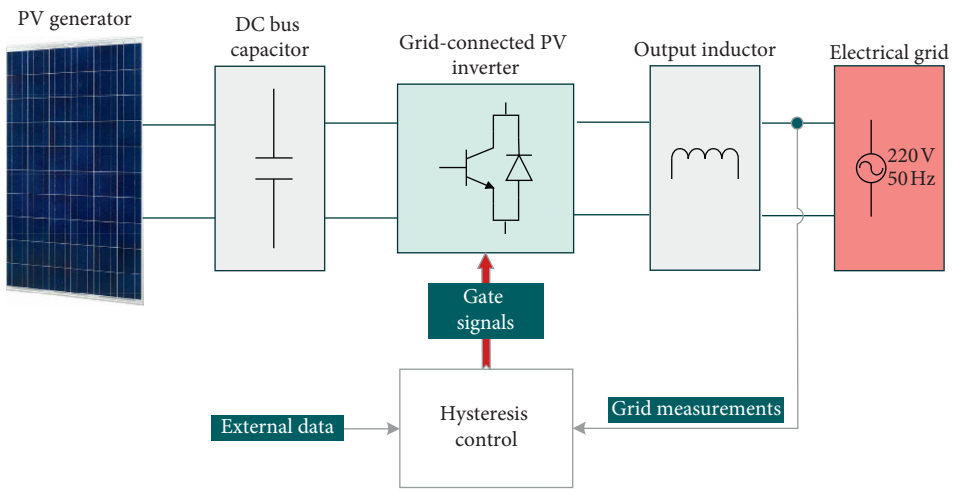

Figure 1: Overview of a grid-connected PV energy conversion system.

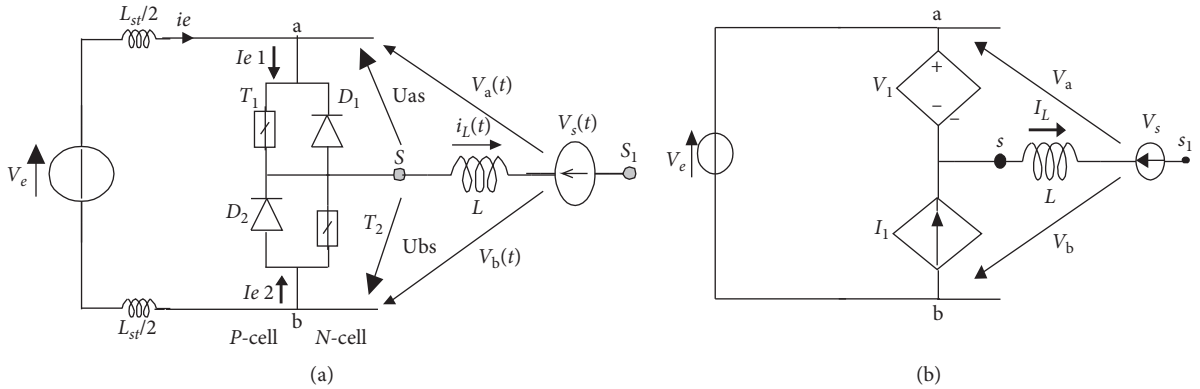

Figure 2: (a) The PWM-switch; (b) the corresponding averaged model.

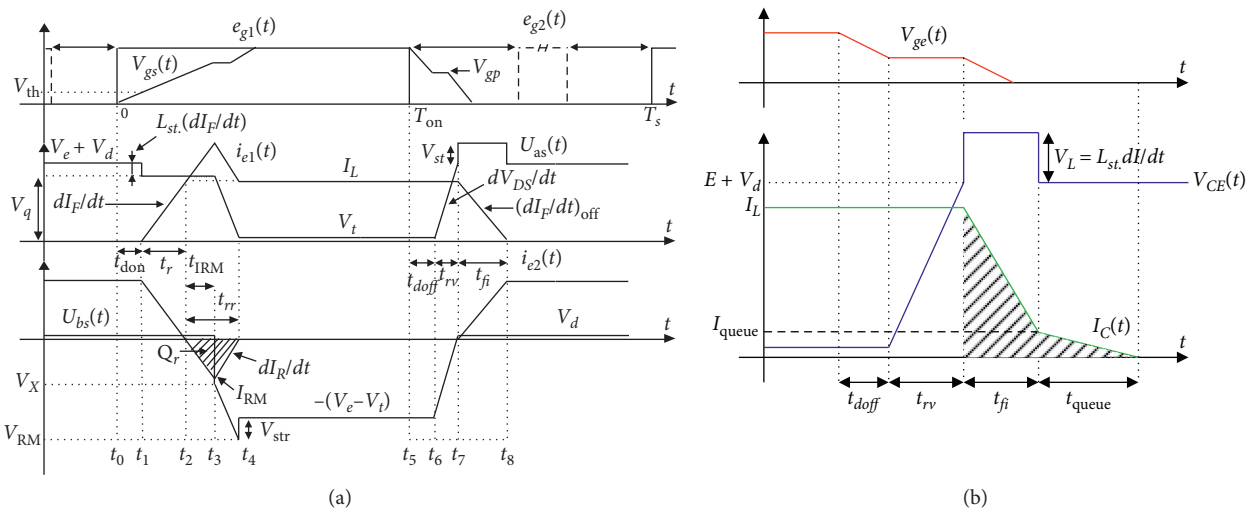

Figure 3: Adopted switching characteristics in the PWM-switch of (a) MOSFET and diode over a switching period. (b) IGBT during blocking commutation.

The use of hysteresis control with model based on electrical circuit does not pose any problems since the switches are controlled by the generic gate signals (high for conduction state and low for blocking one). However, this is not the case for the average models where switches are monitored by duty cycle. This developed method is explained in more detail in [25, 26].

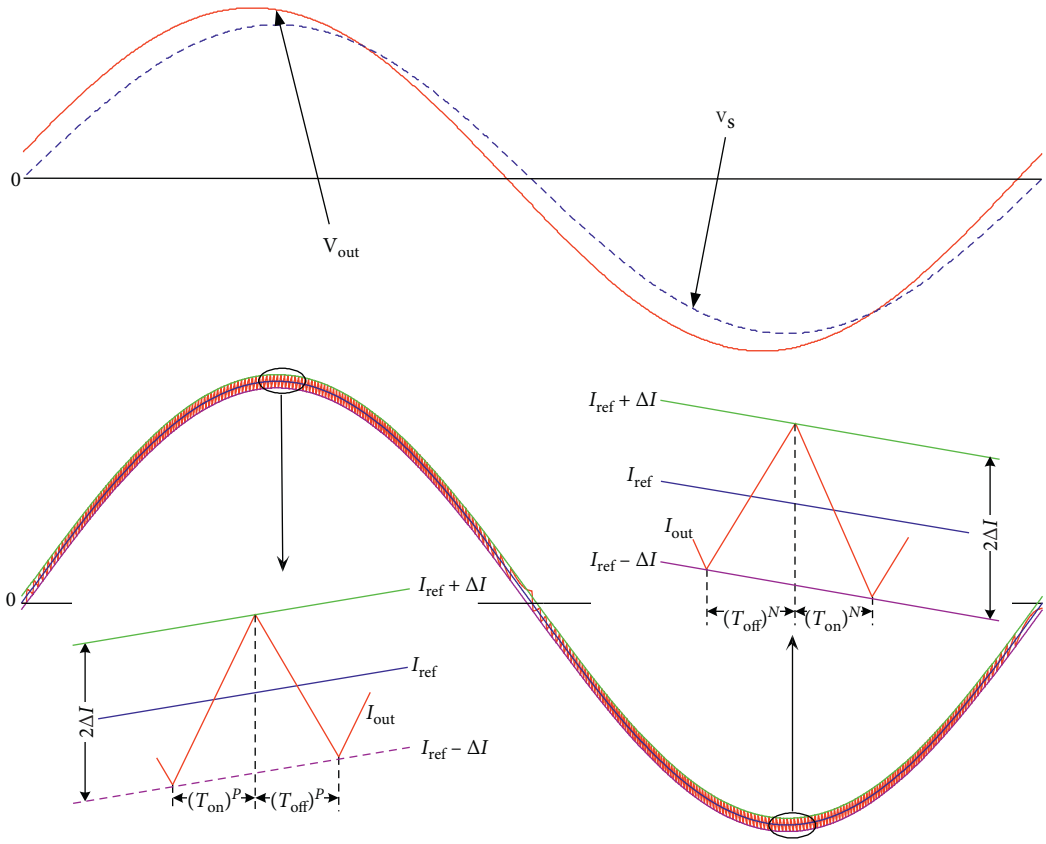

Figure 4: Principle of hysteresis current control strategy.

2.3. Maximum Switching Frequency. One of the most critical parameters in a power converter is the switching frequency which can vary from a few kHz to a few MHz (20 kHz–2 MHz). A high value reduces the size of associated components such as inductors, transformers, resistors, and capacitors. On the other hand, the switching frequency directly affects power dissipation in semiconductor devices (diodes, MOSFETs, IGBTs, etc.), inductive and capacitive elements, and electromagnetic interference.

Moreover, when discussing the switching frequency of a semiconductor, it is obvious to be concerned with its internal temperature since these two parameters are interdependent. In fact, an uncontrollable increase in the switching frequency can lead to an unexpected rise in temperature and subsequently to the instantaneous failure of the component and, at best, a decrease in its life cycle. For this reason, an estimation of the maximum switching frequency $f_{s,\max}$ as function of power system specifications should be done.

3. Elitist Nondominated Sorting Genetic Algorithm

Genetic algorithms are random optimization techniques derived from approximate modeling of the natural evolution of races. They are based on the principle of species evolution mentioned by Darwin which shows how, since their appearance, species have been able to reproduce in an innovative and flexible way to better adapt to the environment, by allowing only individuals well adapted to their environment to evolve [27]. The basic principle, although simple, is nevertheless powerful.

One of the most suitable genetic algorithms for solving multiobjective optimization problems is NSGA-II introduced by Deb et al. in [28, 29]. Figure 5 is a schematic explanation of this algorithm process. NSGA-II first randomly creates an initial population of N individuals, each of whom is characterized by a set of design parameters (Figure 5(a)). Based on objective functions, the NSGA-II ranks the N individuals using the concept of "nondomination". In fact, all individuals are classified into groups of different levels of nondominance in the fitness space (Figure 5(b)). In addition to the fitness assignment, it is also necessary to maintain the diversity of the population in the nondominated front. For this, a density-estimation metric, known as crowding distance, is calculated for each individual (Figure 5(c)). After individuals ranking and their crowding distances allocation, the binary tournament selection is affected according to their objective function and their crowding distance. NSGA-II first selects parents from the 1st rank in the current generation population. Then, individuals with a greater crowding distance are selected as parents while those with a smaller distance are rejected (Figure 5(d)). The selected parents produce the corresponding offspring through the crossover and mutation operators. The newly produced offspring population is then merged with the current generation population (Figure 5(e)). Finally, an elitist process is carried out on the

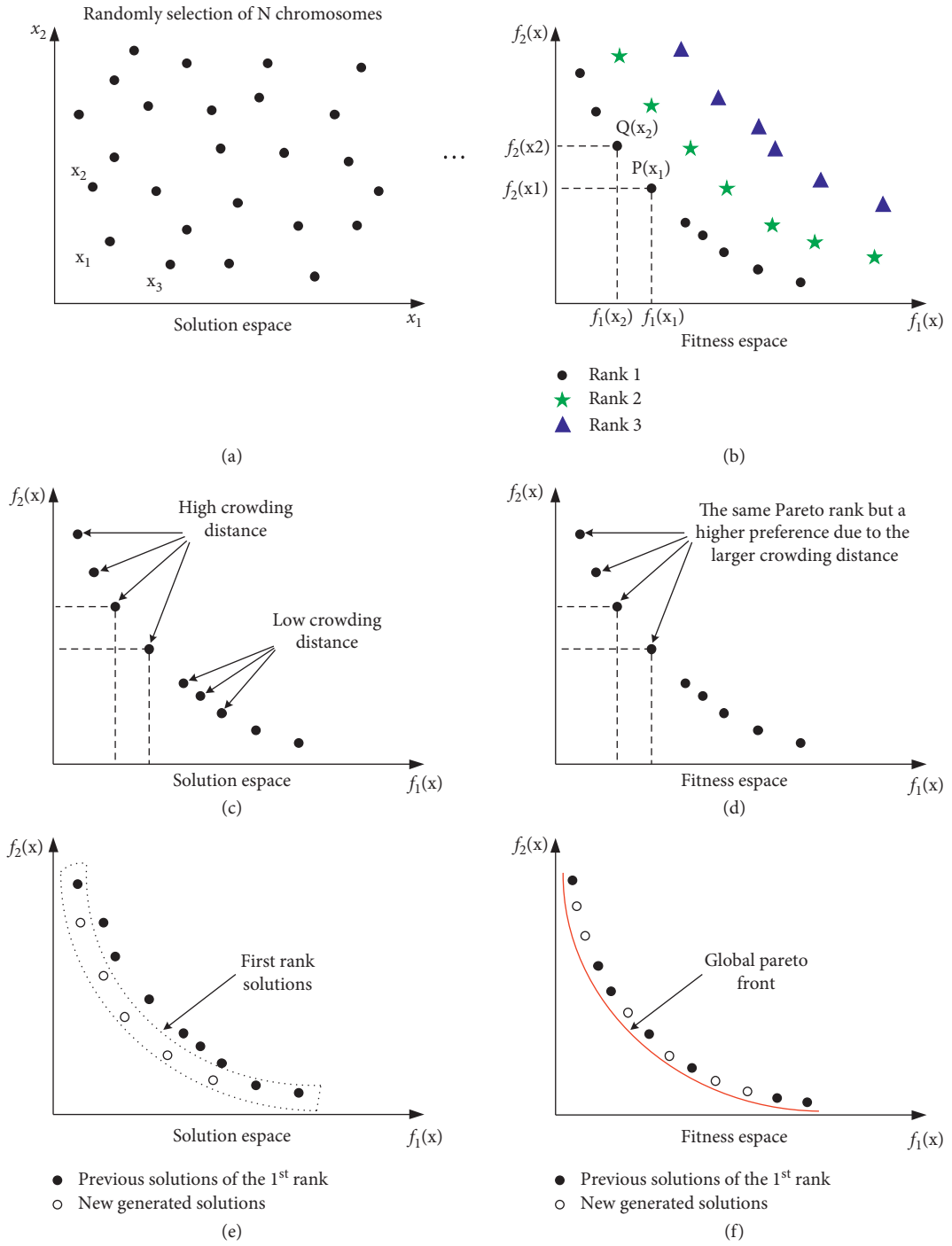

Figure 5: Schematic representation of NSGA-II.

combined population in order to identify the best solutioxns, based on two criteria: the individuals' ranks and their crowding distances. The best solutions of the current generation are the individuals of the next generation. Then, all the above processes (the binary tournament selection, crossover operator, mutation operator, etc.) are iterated until the defined maximum number of generations is reached. Finally, NSGA-II produces a set of N optimal solutions towards a global Pareto front (Figure 5(f)). Once the Pareto front is available, the decision maker should calculate the distance between each Pareto solution and the ideal solution as follows:

$$d_i = \sqrt{\left(\frac{F_{i_1} - F_1^{\min}}{F_1^{\min}}\right)^2 + \left(\frac{F_{i_2} - F_2^{\min}}{F_2^{\min}}\right)^2 + \cdots + \left(\frac{F_{i_m} - F_m^{\min}}{F_m^{\min}}\right)^2}, \tag{4}$$

where $d_i\,(i = 1 \ldots N;\ N$: population size) is the distance between the ideal point and the i_{th} individual,

$\{F_{i_1}, F_{i_2}, \ldots, F_{i_m}\}$ $(m \geq 2)$are the problem objectives for the i_{th} Pareto optimal individual, and $[F_1^{\min}, F_2^{\min}, \ldots, F_m^{\min}]^T$is the ideal objective vector.

And then the closest individual to ideal vector is defined as the best solution.

4. Discrete Optimization Problem Formulation

Opposed to continuous optimization where all problem parameters are continuous quantities, the discrete optimization deals with choosing an optimal solution using either pure discrete design variables or a discrete and continuous combination. The appropriate process for grid-tied PV inverter optimization problem with discrete design parameters is illustrated in the flowchart in Figure 6. As presented, the NSGA-II identifies the design parameters from databases that are then used in the simulation model to calculate the constraints of the problem and determine the values of the objective functions that are then returned to the genetic algorithm for evaluation. This will be repeated for each individual in the population and for each generation until the maximum number of generations is reached.

Thus, the optimization problem can be formulated by the following general system:

$$\min_{x \in R^4} \left(\text{Losses}(x),\ \text{Cost}(x),\ \begin{pmatrix} \text{Losses}(x) \\ \text{Cost}(x) \end{pmatrix} \text{or} \begin{pmatrix} \text{Losses}(x) \\ \text{Volume}(x) \\ \text{Cost}(x) \end{pmatrix} \right),$$

$$\text{under} \begin{cases} THD \leq 5\% \\ f_{s,\max} \leq f_{s,\text{limit}} \\ x \in X \end{cases} \text{with } x = \begin{pmatrix} \Delta I\,(\text{continuous}) \\ L\,(\text{discrete}) \\ T\,(\text{discrete}) \\ D\,(\text{discrete}) \end{pmatrix},$$

$$X(N \times 4) = \begin{pmatrix} 0.2 & L_{i \in [1,N_L]} & T_{i \in [1,N_T]} & D_{i \in [1,N_D]} \\ \vdots & \vdots & \vdots & \vdots \\ \Delta I & L & T & D \\ \vdots & \vdots & \vdots & \vdots \\ 1.5 & L_{j \in [1,N_L]} & T_{j \in [1,N_T]} & D_{j \in [1,N_D]} \end{pmatrix}. \tag{5}$$

T and D are, respectively, the transistor and the diode. N_L, N_T, and N_D are the sizes of the database of inductances, transistors, and diodes, respectively.

4.1. Design Parameters. These are the numerical quantities that define each individual and are modified during the optimization process to achieve fitness functions while meeting the constraints. The design parameters of our optimization problems with discrete variables are well described in Table 1. Component databases are defined as an input to the optimization algorithm. They are implemented from text files to facilitate updating, maintenance, and setup if necessary. The databases of power transistors (IGBT, MOSFET), freewheel diodes, and output inductors required for the design and available on the market, their technical characteristics, and their associated unit costs are given in Tables 2–4.

4.2. Problem Constraints. Depending on the technical characteristics of the system to be studied, limits on its operation are always imposed and must be taken into account when formulating an optimization problem. In the case of grid-tied PV inverter optimization, constraints on the quality of the output power and the switching frequency of the converter must be considered. Thus, two constraints are defined: the total harmonic distortion of output current which should not exceed 5% in normal operation and the maximum switching frequency $f_{s,\max}$ which should not overpass a limit value $f_{s,\lim}$ chosen equal to 50 kHz.

4.3. Fitness Functions. Three contradictory objective functions are taken into consideration which are the power losses of the grid-tied inverter, its volume, and its cost. In fact, the losses of a power converter are very significant since they characterize its conversion efficiency. The volume specifies the space to be allocated by the converter in relation to the other equipment of the PV installation so it must be taken into account because it is not profitable enough to design a very large converter even if its efficiency is the best or its price is the lowest. The cost describes the economic aspect of the converter that needs to be considered without degrading the other performances.

Power losses are caused mainly by the semiconductor devices and the output inductor. Semiconductor power losses are given by (2) and (3) and the load inductor losses are defined by the following:

$$P_L = P_{cu} + V_L P_{\text{core}}. \tag{6}$$

P_{cu} are the inductor copper losses and can be expressed by

$$P_{cu} = R_{\text{DC}} I_{L,rms}^2. \tag{7}$$

R_{DC} is the inductor DC resistance obtained from the database of inductors, and $I_{L,rms}$ is the rms value of the output current.

V_L is the volume of output inductor and is determined from the database of inductors while P_{core} are the time-average power losses per unit volume which are assumed to be given by the well-known Steinmetz equation [30–32]:

$$P_{\text{core}} = K F^{\alpha} \widehat{B}^{\beta}. \tag{8}$$

We notice that all the inductors values in Table 4 are supposed to be independent of frequency.

$\widehat{B}$ is the peak induction of sinusoidal excitation with frequency F and K, α, and β are Steinmetz parameters.

Thus, the total power losses of the inverter can be defined as

$$P_{\text{Inverter}} = P_L + 4\left(P_{\text{transistor}} + P_{\text{diode}}\right). \tag{9}$$

The volume of the DC/AC converter for purely electrical optimization problem is mainly due to the inductor volume V_L and the DC-link capacitor volume V_{Cap}:

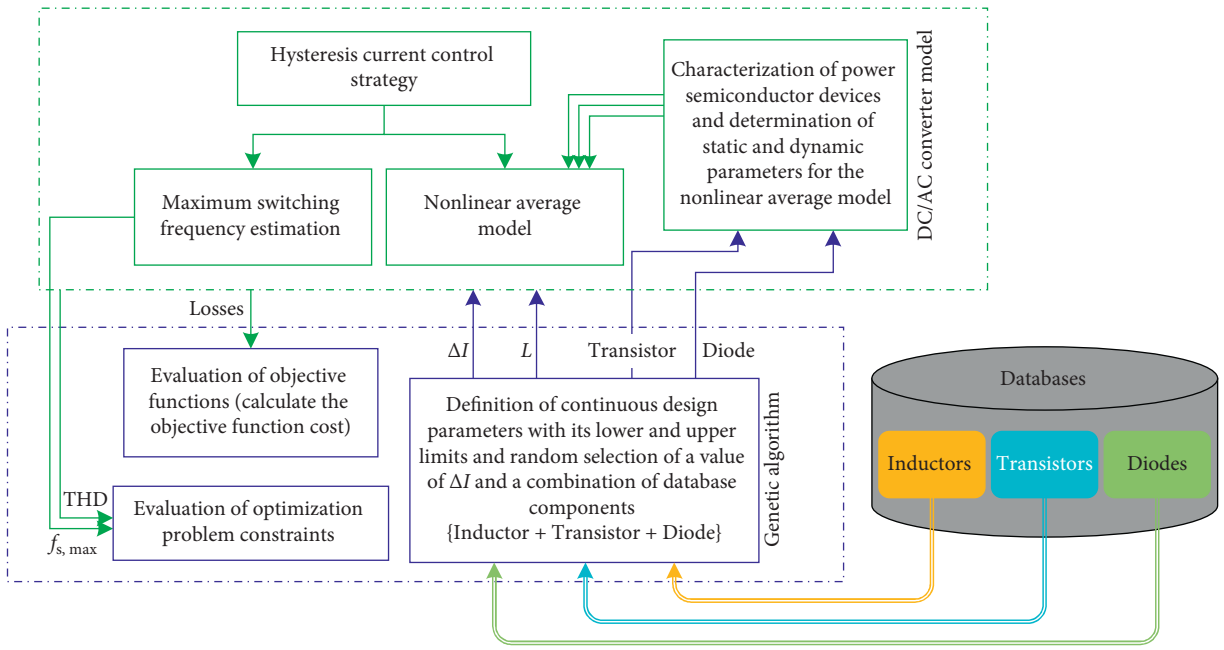

Figure 6: Optimization problem flowchart with discrete design variables.

Table 1: Design parameters.

Parameter	Description	Type	Limits
ΔI	Output current ripple	Continuous	$[2\%I_{\text{ref}}, 15\%I_{\text{ref}}]$
L	Output inductor	Discrete	[1.5 mH, 15 mH]
Transistor	IGBT or MOSFET	Discrete	15 A/650 V
Diode	Freewheeling diode	Discrete	15 A/600 V

$$V_{\text{Inverter}} = V_L + V_{\text{Cap}}. \tag{10}$$

The total cost of the DC/AC converter is the sum of the prices of its components determined from the databases and is given by

$$C_{\text{Inverter}} = C_{\text{Cap}} + C_L + 4\left(C_{\text{transistor}} + C_{\text{diode}}\right). \tag{11}$$

5. Optimization Results

The evolution of single objective optimizations over iterations of power losses, volume, and cost of the grid-connected PV inverter is illustrated in Figure 7. The three fitness functions decrease according to generations and converge towards their minimal values; the inverter power losses (Figure 7(a)) converge towards 32.72 W and the volume (Figure 7(b)) converges towards 645.7 cm^3 while the cost (Figure 7(b)) converges towards 77.94 €.

Table 5 presents the results of the single objective optimizations. For each single-objective optimization problem, the converter optimal design depends on the objective considered, although we have kept the same design variables and optimization constraints in all cases. The first structure is the most efficient because it has the lowest losses, the second is the smallest design which corresponds to the lowest volume, and the third is the most economical, which correctly reflects the concept of minimization.

Nevertheless, single objective optimization treats only one performance criterion and neglects the others. Improving one objective often means degrading others. This is why the concept of compromise is mentioned in optimization in order to obtain an optimal solution as close as possible to the ideal solution which is defined by the optimal solutions of each objective function considered independently (i.e., the monoobjective optimization problems) and which is given in our case for the biobjective optimization problem by the vector:

$$V_{\text{ideal}} = [32.72\,W\ 77.94\,€]^{\text{T}}. \tag{12}$$

The result of biobjective cost vs. losses optimization is shown in Figure 8(a), which is a set of optimal solutions rather than a single optimal one and a trade-off between the inverter losses and its cost. As can be seen, the Pareto front is delimited by the two points "A" and "B." The first solution is the most efficient of all Pareto optimal solutions but it is the most expensive, whereas the second has the highest power losses but it is most economical. The choice of one solution or another depends on the preferences of the designer and the application for which the converter will be used. However, if the best of the best solutions is desired, the closest solution to the ideal one must be taken, which is indicated in Figure 8(a) and its characteristics are given in Table 6.

To go further and to have a more powerful inverter, we consider the triobjective optimization problem which aims to minimize power losses, volume, and cost in order to obtain a structure closer to the ideal one defined by

$$V_{\text{ideal}} = \left[\ 32.72\,\text{W}\ \ 645.7\,\text{cm}^3\ \ 77.94\,€\ \right]^{T}. \tag{13}$$

Table 2: Power transistor database.

Transistor	Description	Nonlinear averaged model parameters										Cost (€)
		$R_{t_{on}}(\Omega)$	V_{t_0}(V)	R_g (Ω)	e_g (V)	V_{th} (V)	V_{gsp} (V)	C_{iss} (pF)	C_{rss} (pF)	g_{fs} (S)	$\frac{dI_F}{dt}$ (A/μs)	
SiHA22N60AE	MOSFET (12 A; 600 V)	0.66	0	9.1	10	3	7.42	1451	13.9	4.8	333.3	1.55
FCPF165N65S3L1	MOSFET (12.3 A; 600 V)	0.51	0	4.7	10	3.5	5.45	1415	9.5	12	452.4	4.41
FCB20N60F	MOSFET (12.5 A; 600 V)	0.76	0	25	10	4	6.32	2370	33.3	17	142.9	4.62
FMV20N60S1	MOSFET (12.6 A; 600 V)	0.11	0	27	10	3	5.25	1470	2.4	17.5	250.0	6.16
FCP190N60	MOSFET (12.7 A; 600 V)	0.63	0	4.7	10	3	4.3	2220	8.4	21	1000.0	2.93
IRG7SC12FPbF	IGBT (13 A; 600 V)	0.04	1.42	47	15	6	9.23	880	7.2	6.2	400.0	1.34
IRFP460BPbF	MOSFET (13 A; 500 V)	0.72	0	4.3	10	3	5.45	4200	10	13	339.0	2.02
SiHP22N60E	MOSFET (13 A; 600 V)	0.50	0	4.7	10	3	6.2	1920	13.7	6.4	407.4	1.59
SPW20N60S5	MOSFET (13 A; 600 V)	0.12	0	3.6	10	4.5	8	3000	7	12	800.0	4.15
FCH190N65F	MOSFET (13.1 A; 650 V)	0.69	0	4.7	10	4	5.59	2425	9.5	18	909.1	4.03
STGB14NC60K	IGBT (14 A; 600 V)	0.10	1.39	10	15	5.5	9.84	760	26.5	3	823.5	1.43
STGD7NC60HT4	IGBT (14 A; 600 V)	0.05	1.53	10	15	4.75	8.44	720	20.8	4.3	823.5	1.63
FCPF150N65F	MOSFET (14.9 A; 650 V)	0.69	0	4.7	10	4	5.7	2810	9.5	22	800.0	5.05
SiHP24N65EF	MOSFET (15 A; 650 V)	0.70	0	9.1	10	3	5.67	2656	13.3	7.2	352.9	2.50
IRGS15B60KPbF	IGBT (15 A; 600 V)	0.03	1.11	22	15	4.5	7.33	850	19	10.6	937.5	2.19
NGTG15N60S1EG	IGBT (15 A; 600 V)	0.02	1.11	22	15	5.5	9.375	1950	22.7	10.1	535.7	1.56
SGP15N60	IGBT (15 A; 600 V)	0.05	1.3	21	15	4	6.96	800	44.1	10.9	652.2	1.48
IXYP15N65C3	IGBT (15 A; 650 V)	0.05	1.07	20	15	4.75	9.4	583	13.3	8.5	750.0	2.13

Table 3: Power diode database.

Diode	Description	Nonlinear averaged model parameters		Cost (€)
		$R_{d_{on}}$ (Ω)	V_{d_0} (V)	
12EWH06FN-M3	12 A/600 V	0.05	1.29	0.49
15EWH06FN-M3	15 A/600 V	0.02	1.33	1.11
ETL1506-M3	15 A/600 V	0.01	0.88	1.14
15EWX06FN-M3	15 A/600 V	0.04	1.81	0.5
ETX1506FP-M3	15 A/600 V	0.08	1.68	1.19
ETU1506-M3	15 A/600 V	0.02	1.18	1.23
ETX1506-M3	15 A/600 V	0.06	1.87	1.23
ETH1506-1-M3	15 A/600 V	0.03	1.42	1.35
15ETL06PbF	15 A/600 V	0.01	0.87	1.36
15ETH06PbF	15 A/600 V	0.04	1.34	1.42
15ETX06PbF	15 A/600 V	0.05	1.73	1.45
HFA15PB60-N3	15 A/600 V	0.02	1.39	2.92

Figure 8(b) depicts the Pareto front for the triobjective optimization problem which is delimited by the two points "C" and "D." The first represents the most efficient inverter design based on the components available on the market, while the second is the most economical with a lower volume. The switching frequency at point "D" is higher than at point "C," resulting in higher power losses, but the volume and cost decrease because they are inversely proportional to the frequency. The best inverter structure for this optimization problem is detailed in Table 6.

To validate the approach using discrete variables, a comparison for the same triobjective optimization problem with the one using continuous parameters is presented in Figure 9. As shown, the result of the continuous

Table 4: Output inductor database.

L (mH)	R_{DC} (Ω)	Volume (cm^3)	Cost (€)
1	0.009	23.485	5.51
2	0.018	23.485	5.51
2.5	0.011	17.108	7.12
3	0.027	46.97	11.02
3.3	0.0084	80.08	13.32
3.5	0.02	40.593	12.63
4	0.036	46.97	11.02
4.3	0.0174	103.565	18.83
4.5	0.029	40.593	12.63
5	0.022	34.216	14.24
5.3	0.0264	103.565	18.83
5.8	0.0194	97.188	20.44
6.3	0.0354	127.05	24.34
6.6	0.0168	160.16	26.64
7	0.04	57.7	19.75
7.6	0.0258	183.645	32.15
8.6	0.0348	183.645	32.15
9.1	0.0278	177.268	33.76
10	0.1	709.93	36.68
11	0.109	733.415	42.19
12	0.118	733.415	42.19
12.5	0.111	727.038	43.8
13.3	0.1084	790.01	50
14	0.298	756.9	47.7
14.5	0.129	750.523	49.31
15	0.062	2098.5	119.2
15	0.12	802.944	94.9

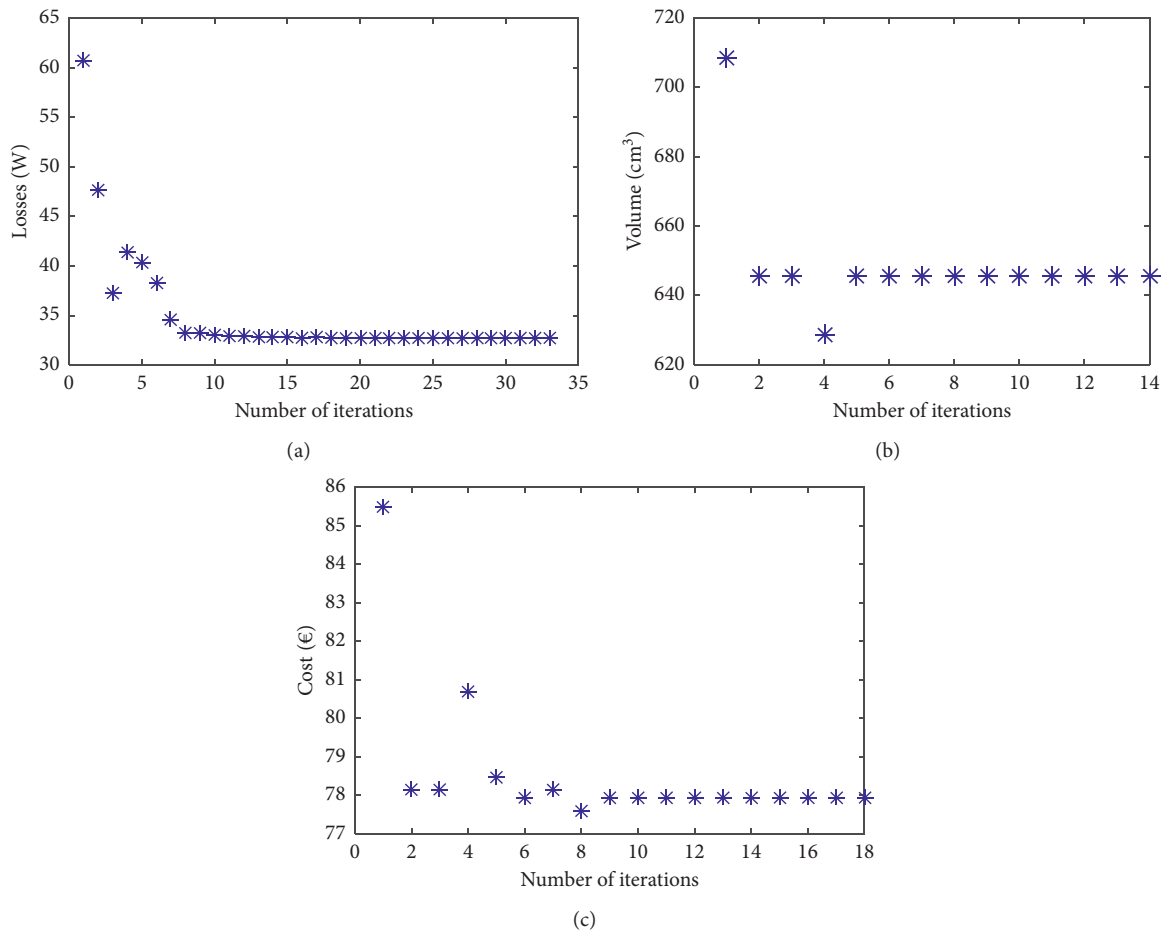

Figure 7: Convergence of the fitness functions according to the number of iterations.

Table 5: Optimal design of the grid-connected inverter for the monoobjective optimization problems.

Optimization problem	Objectives					Variables		Constraints	
	Losses (W)	Volume (cm^3)	Cost (€)	ΔI (A)	L (mH)	Transistor	Diode	THD	$f_{s,max}$ (kHz)
Losses	**32.72**	645.7	98.86	0.556	5	MOSFET SPW20N60S5	ETU1506-M3	0.0477	17.97
Volume	39.59	**645.7**	91.5	0.504	5	MOSFET FCPF165N65S3L1	ETX1506FP-M3	0.0433	19.83
Cost	62.99	628.6	**77.94**	0.426	2.5	IGBT STGB14NC60 K	15EWX06FN-M3	0.039	46.96

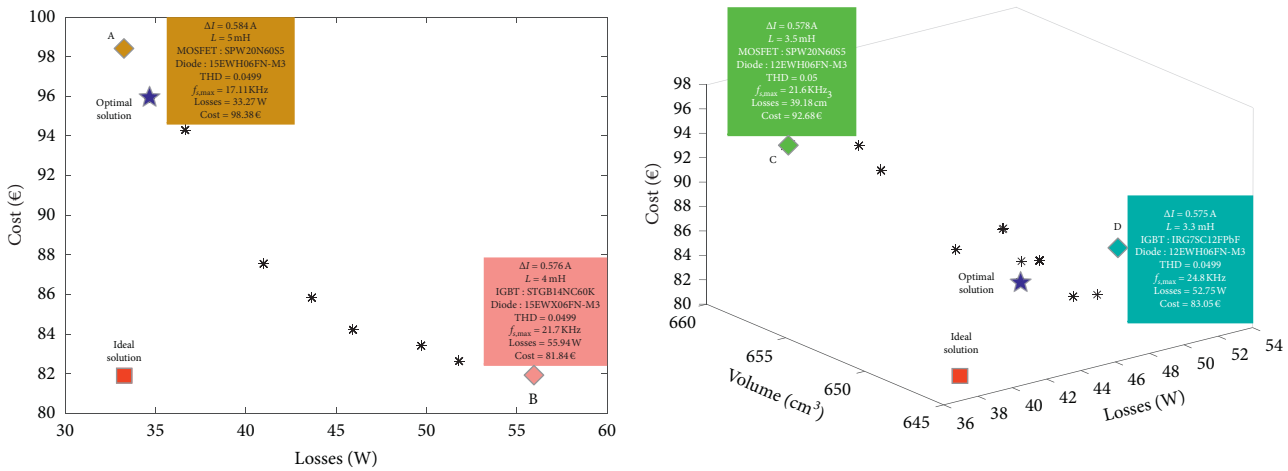

Figure 8: Pareto front of the (a) biobjective optimization problem cost vs. losses. (b) Triobjective optimization problem cost vs. volume vs. losses.

Table 6: Optimal design of the grid-connected inverter for the multiobjective optimization problems.

Optimization problem	Objectives					Variables		Constraints	
	Losses (W)	Volume (cm^3)	Cost (€)	ΔI (A)	L (mH)	Transistor	Diode	THD	$f_{s,max}$ (kHz)
Cost/losses	34.67	—	95.9	0.584	5	MOSFET SPW20N60S5	12EWH06FN-M3	0.0499	17
Cost/volume/losses	41.12	645.7	87.86	0.588	4.5	IGBT			
IXYP15N65C3	15EWX06FN-M3	0.05	17						

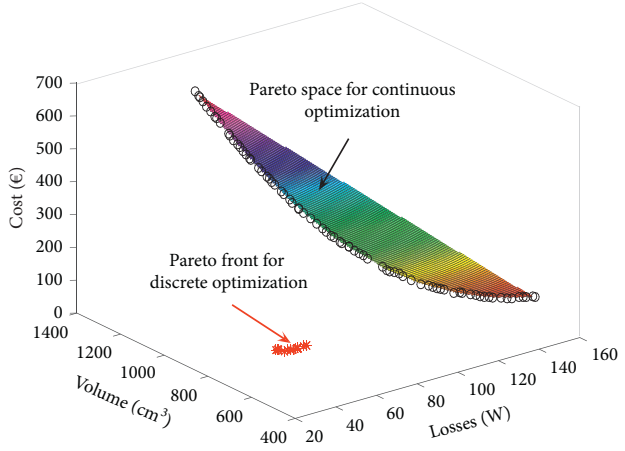

Figure 9: Comparing the Pareto front for discrete triobjective optimization problem to the Pareto space for a continuous one.

optimization problem is a Pareto space that certainly contains unfeasible solutions while the discrete variable problem is a Pareto front where each solution matches a set of components present on the market. In addition, we notice that the discrete variable problem delivers solutions that dominate those of the continuous variable problem so it gives better results. This is mainly due to the use of a well-defined pair (transistor; diode) in the continuous case that limits the optimization task and the attachment to the model used to estimate the costs and volumes of passive components that remains more or less close to reality.

6. Conclusion

The power converter is a key stage in any simple or complex, small or large scale, stand-alone or grid-connected power generation system. Therefore an accurate design of this conversion stage influences the performance of the entire system. This task is too difficult since the power converter is the seat of several physical phenomena (electrical, thermal, electromagnetic, etc.) which leads to the development of the predesign approach of the power converters.

In fact, optimization algorithms are applied to determine the optimal design of the converter before proceeding with its implementation. The purpose of this paper is to exploit genetic algorithms to overcome the difficulties encountered in the design of power converters, to take advantage of the accuracy and speed of nonlinear average models in conjunction with the utility and simplicity of hysteresis current control, and finally, to use the active and passive components available on the market to find the optimal structures of the solar inverter in a grid-connected PV application depending on considered fitness functions. The approach developed in this article will considerably facilitate the design task of power converters for a given application.

Conflicts of Interest

The authors declare that they have no conflicts of interest.

Acknowledgments

This work was funded by King Abdulaziz City for Science and Technology (KACST) (Grant no. 14-ENE2677-10).

References

[1] "BP statistical review of World energy 2019: an unsustainable path," 2019, https://www.bp.com/content/dam/bp/business-sites/en/global/corporate/pdfs/news-and-insights/press-releases/bp-statistical-review-of-world-energy-2019.pdf.

[2] UNEP, *Global Trends in Renewable Energy Investment 2019*, Frankfurt School – UNEP Collaborating Centre for Climate & Sustainable Energy Finance, Nairobi, Kenya, 2019, https://www.connaissancedesenergies.org/sites/default/files/pdf-pt-vue/GTR2019.pdf.

[3] US. Energy Information Administration, *International Energy Outlook 2016*, US. Energy Information Administration, Washington, DC, USA, 2016, https://www.eia.gov/outlooks/ieo/pdf/0484(2016).pdf.

[4] REN21, *Renewable Energy Policy Network for the 21st Century, Renewables 2019 Global Status Report*, REN21 Secretariat, Paris, France, 2019, https://www.ren21.net/wp-content/uploads/2019/05/gsr_2019_full_report_en.pdf.

[5] J. Khan and M. H. Arsalan, "Solar power technologies for sustainable electricity generation - a review," *Renewable and Sustainable Energy Reviews*, vol. 55, pp. 414–425, 2016.

[6] F. Blaabjerg and D. M. Ionel, "Renewable energy devices and systems—state-of-the-art technology, research and development, challenges and future trends," *Electric Power Components and Systems*, vol. 43, no. 12, pp. 1319–1328, 2015.

[7] S. Kouro, J. I. Leon, D. Vinnikov, and L. G. Franquelo, "Grid-connected photovoltaic systems: an overview of recent research and emerging PV converter technology," *IEEE Industrial Electronics Magazine*, vol. 9, no. 1, pp. 47–61, 2015.

[8] V. Khare, S. Nema, and P. Baredar, "Solar–wind hybrid renewable energy system: a review," *Renewable and Sustainable Energy Reviews*, vol. 58, pp. 23–33, 2016.

[9] G. K. Singh, "Solar power generation by PV (photovoltaic) technology: a review," *Energy*, vol. 53, pp. 1–13, May 2013.

[10] S. Chakraborty, M. G. Simões, and W. E. Kramer, *Power Electronics for Renewable and Distributed Energy Systems*, Springer-Verlag, London, UK, 2013.

[11] M. Obi and R. Bass, "Trends and challenges of grid-connected photovoltaic systems - a review," *Renewable and Sustainable Energy Reviews*, vol. 58, pp. 1082–1094, 2016.

[12] O. P. Mahela and A. G. Shaik, "Comprehensive overview of grid interfaced solar photovoltaic systems," *Renewable and Sustainable Energy Reviews*, vol. 68, pp. 316–332, 2017.

[13] L. Hassaine, E. OLias, J. Quintero, and V. Salas, "Overview of power inverter topologies and control structures for grid connected photovoltaic systems," *Renewable and Sustainable Energy Reviews*, vol. 30, pp. 796–807, 2014.

[14] J. Jana, H. Saha, and K. Das Bhattacharya, "A review of inverter topologies for single-phase grid-connected photovoltaic Systems," *Renewable and Sustainable Energy Reviews*, vol. 72, pp. 1256–1270, 2017.

[15] F. Beltrame, H. C. Sartori, and J. R. Pinheiro, "Energetic efficiency improvement in photovoltaic energy systems through a design methodology of static converter," *Journal of Control, Automation and Electrical Systems*, vol. 27, no. 1, pp. 82–92, 2016.

[16] S. E. De Leon-Aldaco, H. Calleja, and J. Aguayo Alquicira, "Metaheuristic optimization methods applied to power converters: a review," *IEEE Transactions on Power Electronics*, vol. 30, no. 12, pp. 6791–6803, 2015.

[17] E. Van Dijik, "PWM-switch modeling of dc-dc converters," *IEEE Transaction on Power Electronics*, vol. 10, pp. 659–664, 1995.

[18] B. Lehman, "Extensions of averaging theory for power electronic systems," *IEEE Transaction on Power Electronics*, vol. 11, no. 4, pp. 542–553, 1996.

[19] A. Ammous, K. Ammous, M. Ayedi, Y. Ounajjar, and F. Sellami, "An advanced PWM-switch model including semiconductor device nonlinearities," *IEEE Transactions on Power Electronics*, vol. 18, no. 5, pp. 1230–1237, Sept. 2003.

[20] A. Slim and A. Anis, "Average modeling of DC-DC and DC-AC converters including semiconductor device non linearities"" in *International Conference on Design and Test of Integrated Systems in Nanoscale Technology (DTIS)*, pp. 384–389, Tunis, Tunisia, September 2006.

[21] S. Abid, K. Ammous, H. Morel, and A. Ammous, "Advanced averaged model of PWM-switch operating in CCM and DCM conduction modes"" *International Review of Electrical Engineering(IREE)*, vol. 2, no. 4, pp. 544–556, 2007.

[22] A. Slim, "Contribution to the simplified modelling of static converters: taking into account thermal phenomena," Unpublished Doctoral Dissertation, University of Sfax, Sfax, Tunisia, 2009.
[23] M. Ebrahimi and S. A. Khajehoddin, "Fixed switching frequency generalized peak current control (GPCC) of DC-AC converters," *IEEE Transactions on Power Electronics*, vol. 32, no. 8, pp. 6605–6616, 2017.
[24] M. Kumar and R. Gupta, "Sampled-time-domain analysis of a digitally implemented current controlled inverter," *IEEE Transactions on Industrial Electronics*, vol. 64, no. 1, pp. 217–227, 2017.
[25] I. Tiss, H. Mejbri, K. Ammous, A. Alahdal, and A. Ammous, "Optimal sizing of single phase DC/AC converter for grid-connected PV applications," in *7th International Renewable Energy Congress (IREC)*, Hammamet, Tunisia, March 2016.
[26] I. Tiss, A. Alahdal, K. Ammous, and A. Ammous, "Design of an optimum single phase inverter for a grid tie PV system," *Universal Journal of Electrical and Electronic Engineering*, vol. 6, no. 4, pp. 223–238, 2019.
[27] M. Gen and R. Cheng, *Genetic Algorithms and Engineering Optimization*, John Wiley & Sons, Inc. Canada, 2000.
[28] K. Deb, S. Agrawal, A. Pratap, and T. Meyarivan, "A fast elitist non-dominated sorting genetic algorithm for multi-objective optimization: NSGA-II," in *Parallel Problem Solving from Nature PPSN VI. PPSN 2000. Lecture Notes in Computer Science*, et al. Vol. 1917, Springer, Berlin, Heidelberg, 2000.
[29] K. Deb, A. Pratap, S. Agarwal, and T. Meyarivan, "A fast and elitist multiobjective genetic algorithm: NSGA-II," *IEEE Transactions on Evolutionary Computation*, vol. 6, no. 2, pp. 182–197, 2002.
[30] J. Muhlethaler, J. W. Kolar, and A. Ecklebe, "Loss modeling of inductive components employed in power electronic systems," in *2011 IEEE 8th International Conference on Power Electronics and ECCE Asia (ICPE & ECCE)*, pp. 945–952, Jeju, South Korea, May 2011.
[31] J. Muhlethaler, J. Biela, J. W. Kolar, and A. Ecklebe, "Core losses under the DC bias condition based on Steinmetz parameters," *IEEE Transactions on Power Electronics*, vol. 27, no. 2, pp. 953–963, 2012.
[32] J. Muhlethaler, J. Biela, J. W. Kolar, and A. Ecklebe, "Improved core-loss calculation for magnetic components employed in power electronic systems," *IEEE Transactions on Power Electronics*, vol. 27, no. 2, pp. 964–973, 2012.